GSH or Palmitate Preserves Mitochondrial Energetic/Redox Balance, Preventing Mechanical Dysfunction in Metabolically Challenged Myocytes/Hearts From Type 2 Diabetic Mice

Carlo G. Tocchetti,[1] Viviane Caceres,[1] Brian A. Stanley,[1] Chaoqin Xie,[2] Sa Shi,[1] Walter H. Watson,[3] Brian O'Rourke,[1] Regina C. Spadari-Bratfisch,[1] Sonia Cortassa,[1] Fadi G. Akar,[2] Nazareno Paolocci,[1,4] and Miguel A. Aon[1]

In type 2 diabetes, hyperglycemia and increased sympathetic drive may alter mitochondria energetic/redox properties, decreasing the organelle's functionality. These perturbations may prompt or sustain basal low-cardiac performance and limited exercise capacity. Yet the precise steps involved in this mitochondrial failure remain elusive. Here, we have identified dysfunctional mitochondrial respiration with substrates of complex I, II, and IV and lowered thioredoxin-2/glutathione (GSH) pools as the main processes accounting for impaired state 4→3 energetic transition shown by mitochondria from hearts of type 2 diabetic *db/db* mice upon challenge with high glucose (HG) and the β-agonist isoproterenol (ISO). By mimicking clinically relevant conditions in type 2 diabetic patients, this regimen triggers a major overflow of reactive oxygen species (ROS) from mitochondria that directly perturbs cardiac electro-contraction coupling, ultimately leading to heart dysfunction. Exogenous GSH or, even more so, the fatty acid palmitate rescues basal and β-stimulated function in *db/db* myocyte/heart preparations exposed to HG/ISO. This occurs because both interventions provide the reducing equivalents necessary to counter mitochondrial ROS outburst and energetic failure. Thus, in the presence of poor glycemic control, the diabetic patient's inability to cope with increased cardiac work demand largely stems from mitochondrial redox/energetic disarrangements that mutually influence each other, leading to myocyte or whole-heart mechanical dysfunction. ***Diabetes*** **61:3094–3105, 2012**

From the [1]Division of Cardiology, Johns Hopkins University School of Medicine, Baltimore, Maryland; the [2]Cardiovascular Research Center, Division of Cardiology, Mount Sinai School of Medicine, New York, New York; the [3]Department of Medicine, Division of Gastroenterology, Hepatology, and Nutrition, University of Louisville, Louisville, Kentucky; and the [4]Dipartimento di Medicina Clinica e Sperimentale, Universita di Perugia, Perugia, Italy.

Corresponding author: Miguel A. Aon, maon1@jhmi.edu.

Received 19 January 2012 and accepted 31 May 2012.

DOI: 10.2337/db12-0072

This article contains Supplementary Data online at http://diabetes.diabetesjournals.org/lookup/suppl/doi:10.2337/db12-0072/-/DC1.

C.G.T., V.C., N.P., and M.A.A. contributed equally to this work.

C.G.T. is currently affiliated with the Division of Cardiology, National Cancer Institute, Pascale Foundation, Naples, Italy.

V.C. is currently affiliated with the Departamento de Farmacologia, Universidade Federal de Sao Paulo (UNIFESP/EPM), Sao Paulo, Brazil.

S.S. is currently affiliated with the Department of Pathophysiology, Harbin Medical University, Harbin, China.

R.C.S.-B. is currently affiliated with the Departamento de Biociencias, Campus Baixada Santista-UNIFESP, Sao Paulo, Brazil.

Diabetic cardiomyopathy is a life-threatening complication of type 2 diabetes (1,2), encompassing systo-diastolic and autonomic dysfunction (3) independent of coronary artery disease or hypertension (3,4). Inefficient glycemic control and sympathetic deregulation contribute to limited exercise capacity and postural hypotension in these patients (5–7). Along with insulin resistance, the pathogenesis of diabetes includes unregulated lipid metabolism, altered adipokine secretion/signaling, and oxidative stress (8). High glucose (HG) and elevated levels of circulating fatty acids (FAs) are prominent traits of type 2 diabetes (9,10) where substrate utilization switches from glucose to FA. The increased uptake/utilization by the heart via β-oxidation (11) provides energy and likely compensates for decreased insulin signaling/glucose metabolism (3).

In patients with poor glycemic control, hyperadrenergic activity may also intervene to compensate for postural hypotension (5,12). This may compound defective glycemic control (13), increasing mitochondrial reactive oxygen species (ROS) levels (14). Oxidative stress associated with obesity, HG, and hyperlipidemia stems from elevated ROS production and/or decreased antioxidant defense. In turn, significant oxidative damage happens in plasma and adipose tissue, as reflected by increased lipid peroxidation and protein carbonylation (15). When unrestricted, this ROS emission may cause insulin resistance (16), and mitochondrial dysfunction is central to these phenomena (14,17). HG and adrenergic stimulation may be additive factors in elevating cardiac oxidative stress in type 2 diabetic subjects (18,19) through increased tricarboxylic acid cycle activity (17,20,21). ROS-mediated cardiac complications in diabetes occur via amplification of HG-induced activation of signaling pathways, leading to different manifestations of the metabolic syndrome (3). Excessive ROS burden augments the mitochondrial propensity to oscillations and mechanical dysfunction in hearts during ischemia-reperfusion injury (22–24). High mitochondrial H_2O_2 outflow and augmented levels of manganese superoxide dismutase are evident in nonstimulated perfused *db/db* hearts (25). Moreover, both acute glucose ingestion and chronic high-fat diet render the rodent or human skeletal muscles more oxidized, with altered tissue glutathione (GSH)/large-capacity GSH (GSSG) ratio and absolute GSH levels (26).

Changes in plasmatic glucose levels, increased FA availability, and alterations of the autonomic nervous balance may unleash simultaneously in type 2 diabetic patients. Mitochondria sense all these changes. Yet, despite evidence

proving the presence of highly oxidizing conditions in cardiomyopathy (14,27), sites of mitochondrial-driven excessive ROS emission remain ill-defined in type 2 diabetes (3,11). Nor is it clear whether impaired energetics and shift in substrates chiefly contribute to alter mitochondrial redox balance, particularly in the presence of increased cardiac workload, due for instance to exercise or postural changes. Finally, it is still undetermined whether alterations in mitochondrial redox/energetic assets are necessary and sufficient to perturb cardiac electro-mechanical coupling in *db/db* myocytes/hearts subjected to combined metabolic/energetic stress.

By use of type 2 diabetic *db/db* myocytes/hearts subjected to combined energetic and redox stress (HG + β-adrenergic stimulation), in this study, we aimed at *1*) unveiling mitochondrial steps liable for energetic impairment and redox imbalance (Fig. 1), *2*) correlating these changes with myocyte/heart mechanical dysfunction due to metabolic/redox challenge, and *3*) testing whether a shift in redox balance may help rescue mitochondrial redox assets, and thus function, in metabolically challenged myocytes/hearts.

RESEARCH DESIGN AND METHODS

Male C57BLKS/J-lepr^{db}/lepr^{db} diabetic (*db/db*; stock number 000642) and nondiabetic C57BLKS/J-lepr^{+}/lepr^{+} (+/+; stock number 000662) mice, 8–10 weeks of age, were obtained from The Jackson Laboratory (Bar Harbor, ME) and housed ad libitum with food and water. For all experiments, animals 10–12 weeks of age were used when *db/db* mice were severely hyperglycemic (28). At the time the mice were killed, wild-type (WT) versus *db/db* body mass (g), heart weight (mg), and blood glucose levels were on average 25 ± 0.6 versus 44 ± 1.4; 183 ± 10 versus 148 ± 6; and 220 ± 9 versus 523 ± 12 mg/dL, respectively. All procedures involving the handling of animals were approved by the Animal Care and Use Committee of the Johns Hopkins University and the Mount Sinai Hospital and adhered to the National Institutes of Health Public Health Service guidelines.

Mitochondrial isolation from murine hearts. Isolation and handling of mitochondria were performed as described previously (29). In mouse heart mitochondria, respiratory control ratios (RCRs; state 3/state 4) of 5 or higher were obtained.

Mitochondrial physiological studies. Respiration was assayed in freshly isolated mitochondria with a high-throughput automated 96-well extracellular flux analyzer (Seahorse XF96; Seahorse Bioscience, Billerica, MA) as described in detail elsewhere (30). In brief, a medium containing (in mmol/L) 137 KCl, 2 KH_2PO_4, 0.5 EGTA, 2.5 $MgCl_2$, 20 HEPES at pH 7.2 and 37°C, with 0.2% FA-free BSA was used. Mitochondria were assayed in polyethyleneimine-coated XF96 plates. After removing the solution of polyethyleneimine, the equivalent of 5–15 μg mitochondrial protein was transferred to each well. The status of the different complexes of the respiratory chain was evaluated with substrates of complex I, II, and IV. Maximal respiratory capacity was analyzed in the presence of 1 mmol/L ADP and 50 μmol/L dinitrophenol. Mitochondrial protein was determined using the bicinchoninic acid method, BCA protein assay kit (Thermo Scientific, Barrington, IL). NADPH, $\Delta\Psi_m$, and H_2O_2 were determined as described elsewhere (29), using the same medium as above for measuring respiration (excluding BSA).

Cardiomyocyte functional and redox studies. The same batch of freshly isolated cardiomyocytes was assayed in parallel for contractility and two-photon imaging.

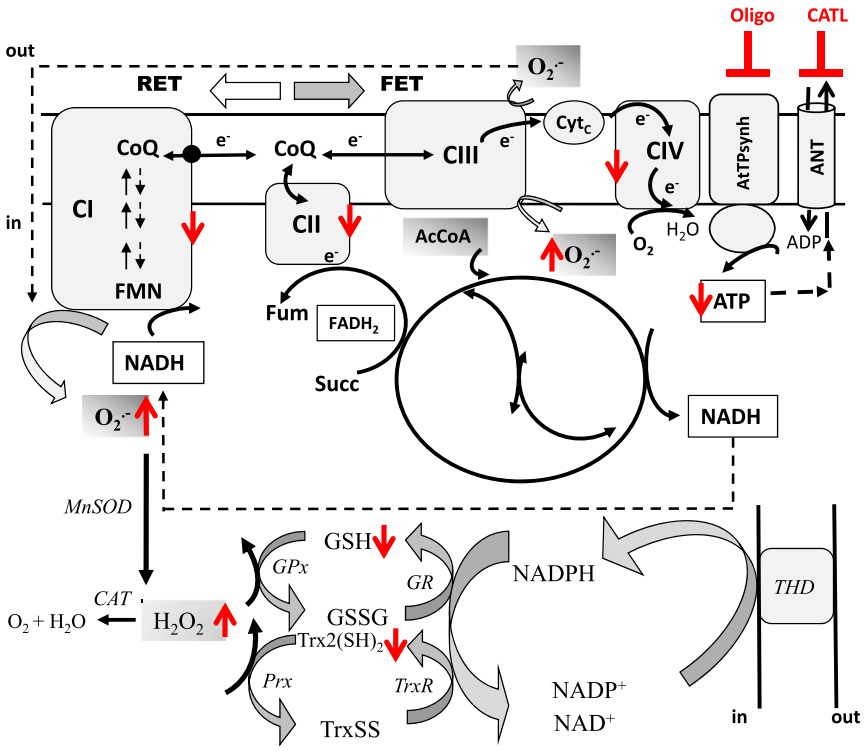

FIG. 1. Major energetic and redox pathways in mitochondria. The scheme shows the respiratory complexes (I–IV), the ATP synthase (ATPsynth), and the ANT in the inner mitochondrial membrane. Also displayed are the major sites of superoxide ($O_2^{\cdot-}$) production and its conversion to H_2O_2 by manganese superoxide dismutase (MnSOD), the tricarboxylic acid cycle, and the H_2O_2 scavenging pathways in the matrix. $O_2^{\cdot-}$ can be produced by complexes I and III (CI and CIII) of the electron transport chain through FET or RET, which depends on NADH- or FADH-linked substrates such as G/M or Succ, donating electrons to complex I or II, respectively. FET and RET, the two main modes of electron transport known, produce markedly different ROS overflow (RET→FET) (29). In RET, electrons flow from complex II to I instead of complex III, which occurs in mitochondria oxidizing high amounts of Succ, but FET is considered the physiological mode. The NADPH/$NADP^+$ coupled with the highest (negative) redox potential (approximately −360 to −400 mV) is the main electron donor of the large-capacity GSH (GSSG) and the Trx (Trx[SH]$_2$, TrxSS) systems responsible for scavenging H_2O_2 via GSH peroxidase (GPx) and peroxiredoxin (Prx) enzymes, respectively. Highlighted in red are the increased (↑: $O_2^{\cdot-}$, H_2O_2, and TrxSS) or decreased (↓: ATP, GSH, and respiratory complex I, II, and IV) levels or activity found after two-photon microscopy imaging of intact cardiomyocytes, contractile measurements, and bioenergetic, redox, and ROS measurements in isolated mitochondria from *db/db* mice. Oligomycin (Oligo) or carboxyatractyloside (CATL) inhibits the ATP synthase or the ANT (indicated by blunted red bars), blocking the state 4→3 transition and mimicking the dysfunctional energetic-redox phenotype shown by *db/db* mice hearts (Fig. 3). AcCoA, acetyl-coenzyme A; CAT, catalase; CIV, respiratory complex IV; CoQ, coenzyme Q; Cyt$_c$, cytochrome c; FMN, flavin mononucleotide; Fum, fumarate; GR, glutathione reductase; THD, transhydrogenase.

Two-photon microscopy. Experiments with intact cardiomyocytes were performed at 37°C in a thermostatically controlled flow chamber mounted on the stage of an upright microscope (Nikon E600FN) attached to a multiphoton laser scanning system, as described previously (31). Cells were loaded with fluorescent probes and imaged as previously described (29,31) (Fig. 2, legend).

Sarcomere shortening and calcium transients. Myocytes were isolated as previously described (32). After isolation, cells were placed in a perfusion chamber with a flow-through rate of 2 mL/min. Sarcomere shortening was assessed by real-time imaging, and whole-cell Ca^{2+} transients by Fura 2-AM fluorescence using an inverted fluorescence microscope (Nikon TE2000) and IonOptix (Myocam) software (32).

Assay of the functional activity of the thioredoxin reductase/thioredoxin system in intact mitochondria. The functional activity of the thioredoxin reductase (TrxR2)/thioredoxin (Trx2) system was monitored in intact mitochondria through the redox status of Trx2 (33). To determine the proportion of reduced and oxidized Trx2, a redox Western blot was performed as described previously (33,34). The redox potential of the Trx2 redox couple was quantified through the Nernst potential as previously described (33).

Assessment of left ventricular function and coronary tone in Langendorff-perfused WT and *db/db* hearts. After anesthesia, hearts were harvested and the aorta cannulated and retrogradely perfused with Krebs-Henseleit (KH) buffer warmed and gassed with 95% O_2 and 5% CO_2. Hearts were paced at 600 bpm (10 Hz, 4-ms duration, 4 V), and left ventricular (LV) function was monitored with a water-filled balloon connected to a pressure transducer coupled to a continuous data recording system. After stabilization, in addition to LV function parameters, baseline values of coronary perfusion pressure (CPP) were obtained through a side arm of the aortic cannula connected to a separate pressure transducer.

High-resolution optical action potential mapping in ex vivo perfused WT and *db/db* hearts. *db/db* and WT mice, 8–10 weeks of age (n = 13), of either sex were killed, and their hearts were rapidly excised, cannulated, perfused, and placed in a custom-designed imaging chamber. Perfusion pressure was maintained at ~60 mmHg and temperature at 36.5 ± 1°C throughout the entire protocol. Unipolar electrocardiograms were recorded for rhythm analysis using silver electrodes (Grass Instruments). Hearts were stained with di-4-ANEPPS (20 μmol/L) for 5 min, allowing the high-resolution mapping of optical action potentials (APs), and therefore, the measurement of epicardial AP duration (APD), normalized upstroke velocity, and conduction velocity (CV) during steady-state pacing, as previously described (35,36).

Statistical analysis. Data were analyzed with the software GraphPad Prism (version 3; San Diego, CA) or MicroCal Origin. The statistical significance of the differences between groups and treatments was evaluated with two-way ANOVA using Tukey multiple comparison test or with a Student t test (small samples, paired t test with two-tailed P values), and the results were presented as mean ± SEM (95% CI).

RESULTS

***db/db* myocytes exhibit more oxidized redox status under metabolic and energetic stress.** Are changes in redox status occurring in WT and *db/db* myocytes at baseline and after metabolic and redox stress? To answer this question, WT and *db/db* myocytes were loaded with ROS or GSH sensors and imaged with two-photon laser scanning fluorescence microscopy (Fig. 2*A*). We compared NADH, GSH, and normalized ROS levels between groups at baseline and during exposure to stress produced by HG (30 mmol/L glucose) and HG + β-agonist isoproterenol (ISO, 10 nmol/L), with or without the FA palmitate (Palm). At baseline, NADH and GSH levels were comparable between WT and *db/db* myocytes (Gluc 5) (Fig. 2*B* and *C*), and exposing myocytes to HG or HG + ISO determined a progressive GSH oxidation (Fig. 2*C*) in both groups, without affecting NADH (Fig. 2*B*). However, stressing *db/db* myocytes either with HG or HG + ISO led to a more prominent decay of GSH levels compared with WT (Fig. 2*C*), with higher MitoSOX fluorescence (Fig. 2*D*). In fact, during exposure to HG + ISO, $O_2^{\cdot -}$ production in *db/db* myocytes was approximately twofold greater than that in WT cells (Fig. 2*D*), with more elevated, although nonsignificant, CM-DCF fluorescence in both WT and *db/db* myocytes (Fig. 2*E*).

To establish whether changes in substrate availability/utilization by the heart can affect cellular/mitochondrial redox balance, we used Palm in the range of serum concentrations found in type 2 diabetes (37). This FA restored redox balance in *db/db* cardiomyocytes (Fig. 2) in a concentration-independent manner (Supplementary Fig. 1). Under any of the conditions tested, Palm efficiently countered exaggerated ROS emission (15–60-fold, $P < 0.001$), increasing GSH levels (20–40%, $P < 0.001$) in both WT and *db/db*. NADH remained nearly all reduced (~93%) (Fig. 2*B*). Together, these data indicate that stress conditions, such as the HG + ISO regimen, unleash the propensity of the *db/db* heart to build up oxidative stress, whereas the use of Palm may overcome some of these adverse events.

Mitochondrial energetic transition is compromised in the heart from *db/db* animals. What sites are liable for altered redox state in type 2 diabetic hearts subjected to metabolic/energetic stress? To answer this question, we measured mitochondrial respiration, coupling of oxidative phosphorylation (OxPhos), NADH levels, $\Delta\Psi_m$, and rate of H_2O_2 emission as a function of respiration state and electron transport mode in isolated mitochondria from WT and *db/db* hearts. Mitochondrial respiration was first quantified in the presence of substrates of complex I, II, and IV and the coupling of OxPhos under each condition (Fig. 3*A–D*). The dynamic response of mitochondrial NADH and $\Delta\Psi_m$ to 5 mmol/L glutamate/malate (G/M) or 5 mmol/L succinate (Succ) and the specific rate of H_2O_2 emission under forward (FET) and reverse electron transport (RET) were also investigated (Fig. 3 and Supplementary Fig. 2).

First, we found that the basic bioenergetic behavior of mitochondria from WT and *db/db* hearts was noticeably different. The RCR (state 3/4), a measure of the degree of coupling of OxPhos, was markedly decreased at the level of the three main respiratory complexes in *db/db* mitochondria (Fig. 3*A*). In *db/db* mitochondria, a trend to higher values of state 4 respiration was evident in both complex I and II (Fig. 3*B* and *C*). Thus, it is plausible that the overall mechanism of energy transduction is impaired in *db/db* mitochondria, including electron flow and ATP synthesis.

Mitochondria from *db/db* hearts exhibited significantly greater H_2O_2 emission levels, both under FET (Fig. 3*E* and *F*) and RET (Fig. 3*G* and *H*) modes of electron transport. ROS emission during state 4→3 transition decreased less in *db/db* mitochondria, especially during FET, the physiological mode of electron transport (Fig. 3*E*), and in the face of similar mitochondrial NADH and $\Delta\Psi_m$ dynamic response to complex I and II substrates (Supplementary Fig. 2). In RET, the decrease in ROS emission observed during state 4→3 transition, both in WT and *db/db* mitochondria (Fig. 3*G*), is likely due to the pronounced $\Delta\Psi_m$ depolarization elicited by ADP (Supplementary Fig. 2), to which ROS by RET is extremely sensitive (38).

The state 4→3 transition is a fundamental one in mitochondrial physiology, representing the shift from a highly energized (i.e., high $\Delta\Psi_m$) and reduced redox status of low respiration and ATP synthesis to high respiration and ATP synthesis in response to elevated ATP demand (Fig. 3*B–D*, *E*, and *F*) (29,39). Hence, we further investigated whether high ROS outflow during 4→3 transition could be localized at a site other than the respiratory complexes. To mimic the *db/db* phenotype, we inhibited the adenine nucleotide translocator (ANT) (with carboxyatractyloside) or the ATP synthase (with oligomycin) in WT mitochondria, measuring

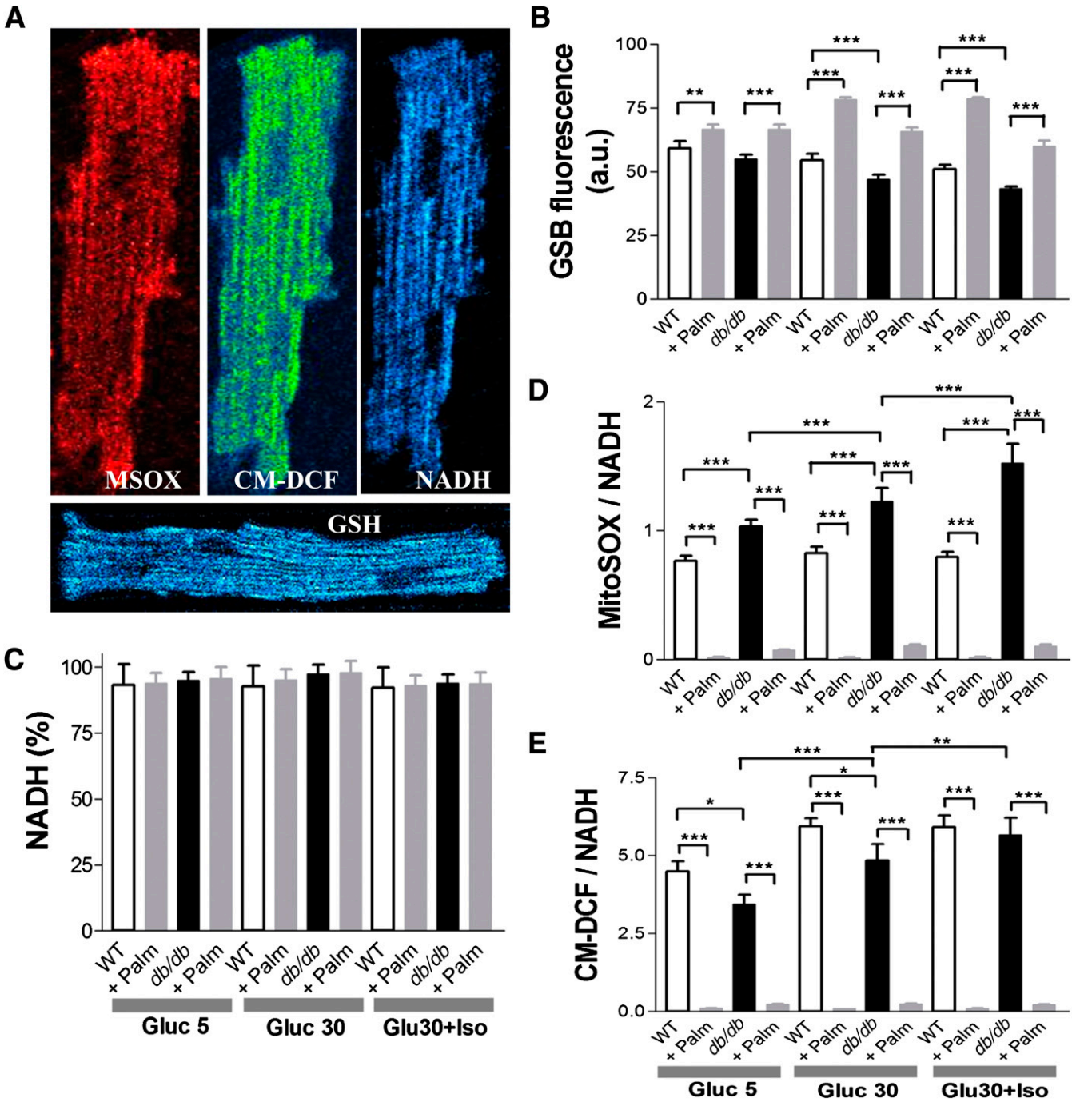

FIG. 2. Imaging of WT and *db/db* cardiomyocyte redox status under normal glucose or HG without or with β-adrenergic stimulation and in the absence or presence of Palm. ROS levels were monitored with the probes 5-(6)-chloromethyl-2, 7-dichlorohydrofluorescein diacetate (CM-H_2DCFDA), MitoSOX (MSOX), and reduced GSH with GSH *S*-bimane (GSB) (31) (all from Invitrogen, Eugene, OR). *A*: Freshly isolated murine cardiomyocytes were loaded with MitoSOX (2 μmol/L, *left panel*) and CM-H_2DCFDA (2 μmol/L, *middle panel*) and imaged with two-photon laser scanning fluorescence microscopy. *B*: GSH was imaged in myocytes loaded with the membrane-permeant indicator monochlorobimane (50 μmol/L, *bottom panel*), reporting the level of GSH as the fluorescent product GSB (31). *C*: NADPH autofluorescence was imaged simultaneously with the ROS probes and used for normalizing MitoSOX (*D*) and CM-H_2DCFDA (*E*) signals. The NADPH signal was calibrated with 1 mmol/L potassium cyanide (KCN) (100% reduction) and 5 μmol/L carbonyl cyanide 4-(trifluoromethoxy)phenylhydrazone (FCCP) (0% reduction or maximal oxidation). Baseline imaging of cells was performed with Tyrode, pH 7.5, containing 1 mmol/L Ca^{2+} and normal (5 mmol/L) glucose, followed by the same solution with 30 mmol/L glucose (HG), in the absence or the presence of 10 nmol/L ISO (Gluc 30 + Iso). The same protocol was repeated in the presence of two Palm concentrations (0.4 or 0.8 mmol/L) for WT or *db/db* (Supplementary Fig. 1). Cardiomyocytes were incubated for 30 or 3 min under HG conditions without or with ISO, respectively. Depicted are the results obtained from paired determinations in two independent experiments with $n = 30$ for each treatment and fluorescent probe. For all fluorescent signals (GSB, MitoSOX, and CM-DCF), WT and *db/db* cardiomyocytes were compared by two-way ANOVA within treatment (e.g., 5 mmol/L glucose) for the absence (control) or presence of Palm. In addition, the normalized ROS signals over NADH (for which fluorescence did not change by treatments) were compared across treatments by two-way ANOVA when Palm was absent or present. *$P < 0.05$; **$P < 0.01$; ***$P < 0.001$. a.u., arbitrary units. (A high-quality digital representation of this figure is available in the online issue.)

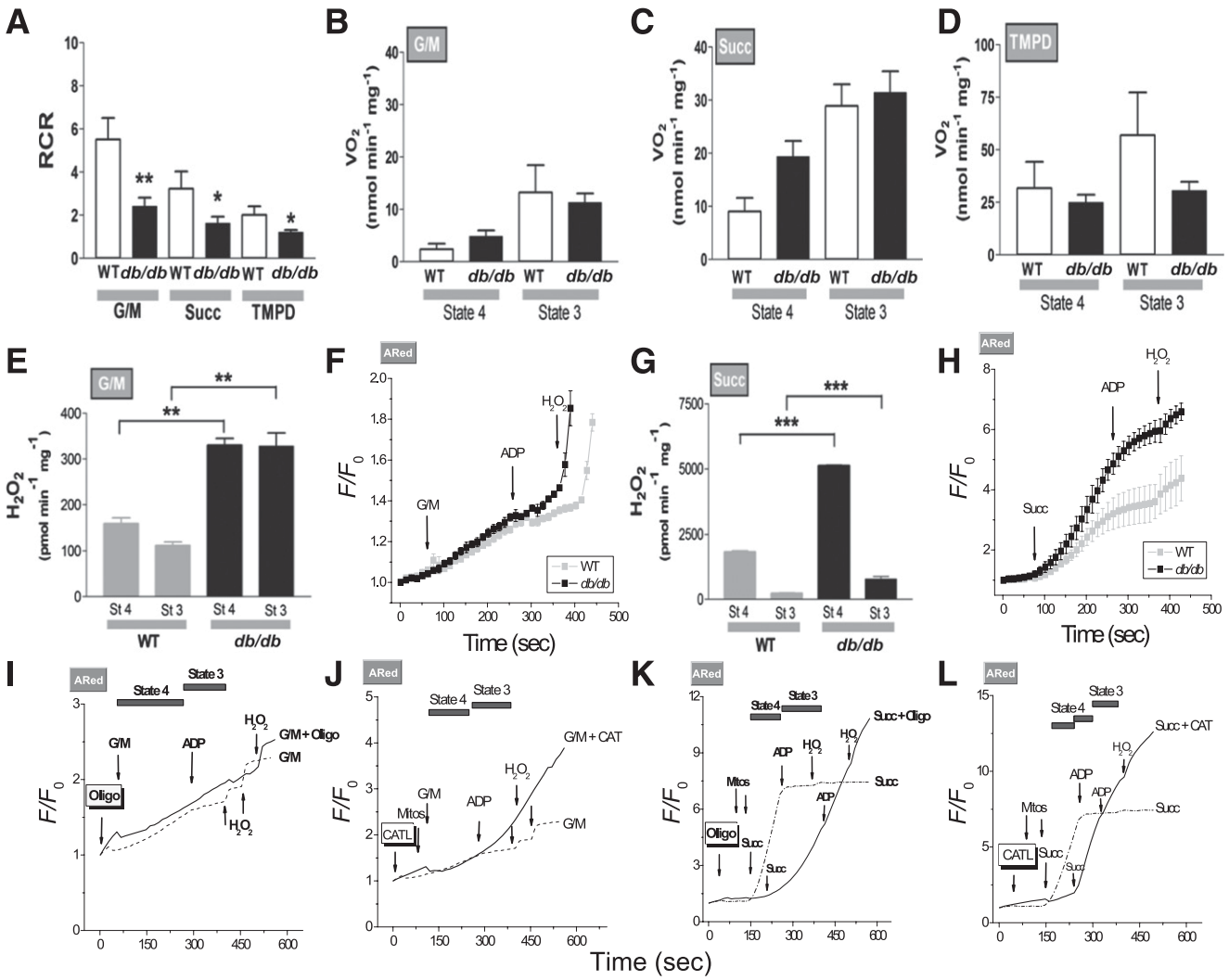

FIG. 3. Energetic and redox behavior of WT and *db/db* mouse mitochondria and blockade of the state 4→3 transition. Respiration in freshly isolated heart mitochondria from WT and *db/db* mouse was analyzed with a SeaHorse XF96 analyzer as described in RESEARCH DESIGN AND METHODS. *A–D*: Mitochondria were assayed under state 4, i.e., substrate but no ADP (48) (sometimes also referred to as state 2) (49), and state 3, i.e., substrate and ADP present, respiration (Vo_2) with substrates from complex I (5 mmol/L G/M) (*B*), complex II (5 mmol/L Succ and 1 μmol/L rotenone) (*C*), and complex IV (0.5 mmol/L *N,N,N′,N′*-tetramethyl-*p*-phenylenediamine [TMPD] and 3 mmol/L sodium ascorbate) (*D*). State 3 was induced with 1 mmol/L ADP in all cases. *A*: The RCR was determined as the ratio of state 3 to state 4. The bars plotted correspond to $n = 8$ replicates from two experiments. Respiratory rates determined in the current study belong to the medium to low range of those reported in the literature. Consequently, we further ascertained the quality of our mitochondrial preparation by assaying citrate synthase activity in WT and *db/db* mitochondrial extracts. The values found compare very well with previous reports (see Supplementary Data). *E–H*: H_2O_2 was monitored with the Amplex Red (ARed) assay. Shown are the results obtained with H_2O_2-specific fluxes (*E* and *G*) or H_2O_2 emission in state 4 or 3 respiration (*F* and *H*) under FET (5 mmol/L G/M) (*E* and *F*) and RET (5 mmol/L Succ) (*G* and *H*). NADH and $\Delta\Psi_m$ were monitored simultaneously with a spectrofluorometer (Supplementary Fig. 2), and O_2 measurements were performed in parallel under similar conditions (*A–D*). Depicted are the normalized ARed traces obtained for WT and *db/db* mitochondria after G/M (*F*), Succ (*H*), and ADP addition, as indicated by arrows. H_2O_2 (50 nmol/L) was added for calibration purposes. The number of samples analyzed was $n = 6$ (two experiments) (*E* and *G*) and $n = 4$ (two experiments) (*F* and *H*). *$P < 0.05$; **$P < 0.01$; ***$P < 0.001$. Mitochondria from WT mouse heart were resuspended and analyzed under FET (*I* and *J*) and RET (*K* and *L*) conditions in a spectrofluorometer for H_2O_2 monitored with ARed or NADH as described in RESEARCH DESIGN AND METHODS. Mitochondria (50–100 μg mitochondrial protein) preincubated with 5 μmol/L oligomycin (Oligo) (*I* and *K*) or 10 μmol/L carboxyatractyloside (*J* and *L*) are indicated by a continuous line, and control mitochondria in the absence of inhibitors are indicated by a dashed line. Additions of substrate (5 mmol/L G/M or 5 mmol/L Succ), 1 mmol/L ADP, or 50 nmol/L H_2O_2 (for calibration) are indicated by arrows. Notice that after Oligo or CATL, H_2O_2 emission continues after ADP (marked) during the transition between states 4→3 of respiration, compared with controls.

H_2O_2 levels in the presence of substrate and ADP. Mitochondrial preparations preincubated with either inhibitor failed to decrease ROS emission when ADP was added, during both FET (Fig. 3*I* and *J*) and RET (Fig. 3*K* and *L*). Thus, impairments in the state 4→3 transition both at the level of electron transport in the respiratory chain and of the ANT and/or ATP synthase are likely liable for the sustained rise in ROS levels in mitochondria from *db/db* hearts.

Trx2 system activity is diminished in type 2 diabetic hearts and can be restored by GSH. Is ROS scavenging capacity impaired in type 2 diabetes, and if so, where? First, we measured the protein expression levels of the main components of the mitochondrial antioxidant system (Fig. 1). Since no differences were found between WT and *db/db* either in isolated mitochondria (Supplementary Fig. 3) or at whole-tissue levels (not shown), we sought for changes in the abundance of the mitochondrial TrxR2/Trx2 system.

Again, no differences were observed (Fig. 4*A*). Therefore, we asked whether changes in Trx2 redox status, i.e., oxidized/reduced (TrxSS/Trx[SH]$_2$), occurred under nonenergized and energized conditions (Supplementary Fig. 2), using G/M as a substrate (FET) (33). This approach revealed marked differences between WT and *db/db* (Fig. 4*B*). At baseline, only 34% of Trx2 was in its reduced status, both in WT and *db/db* (Fig. 4*B*, *top right*). However, substrate addition to energize mitochondria to state 4 led to significantly greater Trx(SH)$_2$ in WT versus *db/db* mitochondria. Trx(SH)$_2$ increased in parallel with NADPH and $\Delta\Psi_m$ when G/M was added (Supplementary Fig. 2). In state 3, Trx2(SH)$_2$ levels remained as high as in state 4. Since the reducing power of Trx2 is determined by the ratio TrxSS/Trx(SH)$_2$, we calculated the latter and expressed it as redox potential. Upon substrate addition to WT mitochondria, the redox potential became more negative, thus more reducing, from -294 ± 5 to -325 ± 2 mV. This increment was less pronounced in mitochondria from *db/db* mice, from -294 ± 5 to -313 ± 2 mV (Fig. 4*B*, *bottom right*). The 12-mV difference in Trx2 redox potential accounts for a significant 2.3-fold rise in the TrxSS/Trx(SH)$_2$ ratio.

Finally, we investigated whether altered Trx2 redox could be reversed by treatment with exogenous GSH ethyl ester (GSHee). Preincubation of *db/db* mitochondria with GSHee caused a significant increase in Trx(SH)$_2$ (from 64 ± 3 to 78 ± 1%), equivalent to a twofold rise in the TrxSS/Trx(SH)$_2$ ratio (Fig. 4*B*, *right*). Noteworthy, these values are comparable to those found in WT Trx(SH)$_2$ levels and similar to those found in state 3. Thus, in addition to their energetic impairment, *db/db* mitochondria exhibit diminished ROS scavenging capacity via the Trx2 system.

Function is impaired in *db/db* myocytes under combined HG + ISO regimen. Next, we tested whether the HG + ISO regimen, which unveiled major redox/energetic deficits in cardiac *db/db* mitochondria, would reverberate on mechanical function and Ca^{2+} transient of myocytes from WT and *db/db* hearts. Changes in the amplitude and kinetics of contractility and Ca^{2+} transients in WT and *db/db* myocytes were measured under normal (5 mmol/L) and HG conditions, in the presence or absence of ISO, with and without Palm at two different concentrations.

Minus Palm. Fractional shortening (FS) and Ca^{2+} transient amplitude/kinetics were similar in WT versus *db/db* myocytes at 5 and 30 mmol/L glucose (Supplementary Tables 1 and 2). Next, we examined the effects of β-stimulation via ISO on *db/db* and WT myocytes. At 5 mmol/L glucose, ISO response was similar in both groups (Table 1). Conversely, HG + ISO unveiled marked differences between *db/db* and WT myocytes: in *db/db*, ISO-induced enhancement of contractility/relaxation was lower, coupled to altered Ca^{2+} kinetics (Table 2 and Fig. 5). These findings

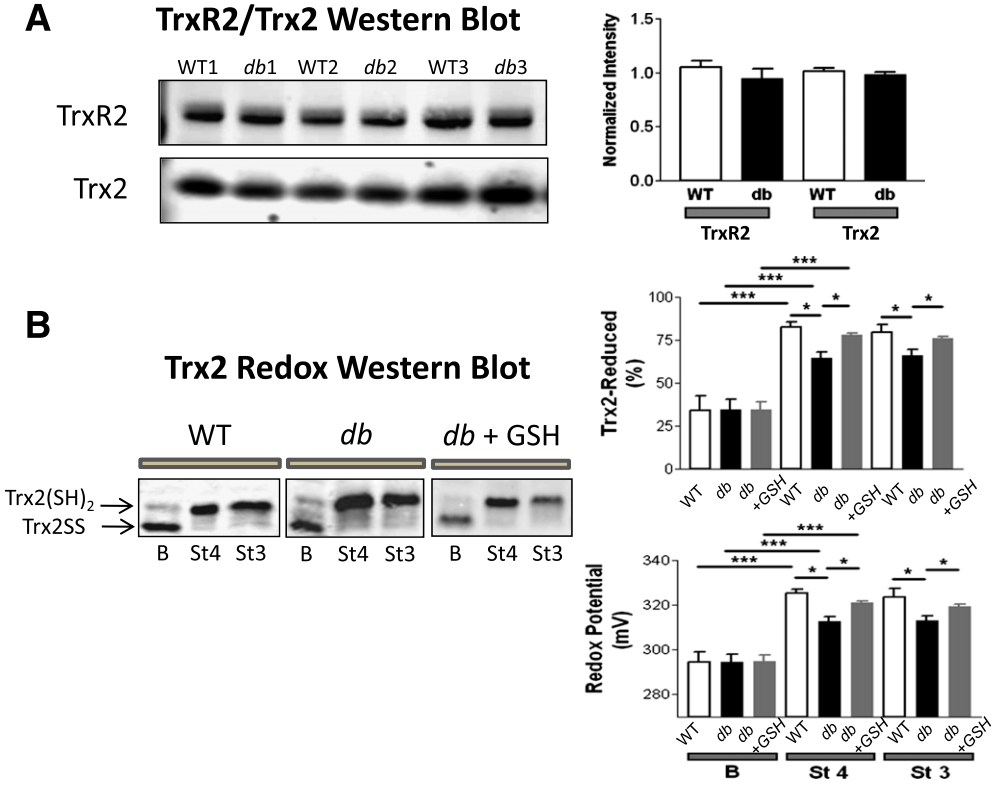

FIG. 4. Abundance, redox status, and response of Trx system from WT and *db/db* mitochondria to preincubation with GSHee. Freshly isolated heart mitochondria from WT and *db/db* mice were handled and analyzed for TrxR2 and Trx2 protein abundance by Western blot (WB) and for Trx-SS and Trx(SH)$_2$ status by redox WB. *A*: Shown are three representative examples (*left*) and the statistical comparison between WT and *db/db* (n = 6 experiments) (*right*). As in Supplementary Fig. 3, protein was normalized to total protein abundance based on Direct Blue 71 staining. Trx(SH)$_2$ and Trx-SS were determined in fresh, active mitochondria (150–200 μg mitochondrial protein), under baseline (nonenergized) (*B*), state 4 (St 4) (5 mmol/L G/M), and state 3 (St 3) (+1 mmol/L ADP) of respiration in paired samples as described elsewhere (33). *B*: Representative redox WB of Trx2 from WT and *db/db* mitochondria (*left*), and the amount of Trx(SH)$_2$ (*right*) (*top*, in %) and redox potential (*bottom*, in mV) comparatively between WT and *db/db* mitochondria, in the absence or presence of GSHee preincubation (3 mmol/L GSHee for 30 min; n = 6 experiments). *P < 0.05; ***P < 0.001.

suggest a deficit in cAMP-dependent protein kinase–mediated enhancement in contractility and Ca^{2+} handling of *db/db* myocytes under HG.

Plus Palm. Under HG, Palm had a significant negative influence on the amplitude of Ca^{2+} transient and sarcomere shortening in *db/db* myocytes at both concentrations tested (Supplementary Tables 1 and 2). Yet, its administration in *db/db* myocytes challenged with HG + ISO improved contractility and Ca^{2+} handling to a higher extent than that seen in WT (Table 2). Palm preserved the cardiomyocyte response to the β-stimulant under HG in myocytes from *db/db* hearts (Fig. 5 and Table 2) as well as in WT and *db/db* cardiomyocytes at 5 mmol/L glucose (Table 1). Thus, Palm is beneficial for *db/db* cardiomyocytes exposed to a concomitant energetic and redox challenge.

GSH or Palm offsets mechanical dysfunction in *db/db* cardiomyocytes challenged with HG and β-agonists. To strengthen the causative link between impaired contractility and the more oxidized redox status of *db/db* cardiomyocytes, and to assess whether a shift in substrates may affect their function under challenging conditions, we tested the impact of cell-permeable GSHee or Palm. Exogenous GSHee offset ISO-mediated changes in ROS and GSH levels of *db/db* cardiomyocytes exposed to HG (Supplementary Fig. 4); all functional indexes recovered to WT levels after GSH (Fig. 5*A–D*). Moreover, GSHee replenished the thiol intracellular pool by ~20%, without significantly changing NADH levels (Supplementary Fig. 4, *insets*), countering, in turn, the rise in ROS levels (Supplementary Fig. 4). To do so, GSHee acted through the reconstitution of the Trx2 pool (Fig. 4), ultimately limiting ROS emission in mitochondria from HG/ISO-challenged *db/db* mice and preventing myocyte mechanical deficiency.

Even more so, Palm significantly improved both contractility and Ca^{2+} handling, beyond the levels required to fully offset HG + ISO adverse effects (Fig. 5*A–D* and Table 2). This beneficial impact was coincident with a more reduced redox status (Fig. 2), both under normal conditions and HG. Thus, in diabetes, FAs may have a role that goes beyond that of energetic providers (11,40); this contention is reinforced by the fact that the impact of GSHee and Palm on myocyte function is not additive (Fig. 5).

WT and *db/db* intact heart LV function and electrophysiological performance. The combined HG + ISO regimen in the absence or presence of Palm uncovered major differences in *db/db* and WT myocyte redox conditions (Fig. 2) and electro-contraction (E-C) coupling impairment (Fig. 5) that were not apparent at baseline (Fig. 2, Table 1, and Supplementary Table 1). These alterations were underlined by mitochondrial energetic/redox alterations (Fig. 3). To evaluate the functional implications of these changes at the whole-heart level, we used Langendorff-perfused mouse hearts and high-resolution optical AP imaging. With the former approach, we evaluated possible changes in LV function and coronary vascular response (CPP) under HG (Fig. 6 and Supplementary Fig. 6) and euglycemia (EG) (Supplementary Figs. 5 and 7) in the absence or presence of ISO and Palm (Fig. 6*A–D* and Supplementary Figs. 5–7*A–D*). As in cardiomyocytes (Fig. 5 and Table 2), whole WT hearts exhibited better LV function versus *db/db* hearts when exposed to HG + ISO (Fig. 6*A–D*). Optical mapping revealed that although HG alone did not alter APD in paced WT and *db/db* hearts, the HG + ISO regimen uncovered important functional differences between groups. Under HG + ISO challenge, there was a significant decrease in both APD50 ($P = 0.019$) and 75 ($P = 0.030$) in *db/db* compared with WT hearts (Fig. 6*E–H* and Supplementary Fig. 8).

Notably, Palm (same concentration as in cardiomyocytes) significantly improved the functional performance of *db/db* hearts exposed to HG + ISO by decreasing CPP and increasing LV-developed pressure (LVDP) concomitantly with the rates of *db/db* heart contraction (dP/dt_{max}) and relaxation (dP/dt_{min}) (Fig. 6*C* and *D*), whereas this FA did not affect WT heart performance (Fig. 6*A–D*). Similar results were obtained at both Palm concentrations tested under HG (Fig. 6 and Supplementary Fig. 6). However, the LVDP, dP/dt_{max}, and dP/dt_{min}, but not CPP, of WT hearts were significantly decreased under EG + ISO at the two Palm concentrations tested (Supplementary Figs. 5 and 7). In essence, Palm improved LV functional performance of hearts from diabetic animals subjected to metabolic/redox challenge.

TABLE 1
Contractility and Ca^{2+} transient kinetics in ventricular myocytes isolated from WT and *db/db* mice, under a normal (5 mmol/L) glucose regimen in the presence of ISO (10 nmol/L), without or with Palm at two different concentrations

	Glucose 5 mmol/L + ISO					
	WT			*db/db*		
	Control	Palm 0.4 mmol/L	Palm 0.8 mmol/L	Control	Palm 0.4 mmol/L	Palm 0.8 mmol/L
FS (%)	9.2 ± 0.4	10.7 ± 1.1	12.4 ± 0.3 ($P < 0.05$ vs. control)	9.4 ± 0.6	10.6 ± 0.6	11.9 ± 1.3
Ca^{2+} transient (%)	43.9 ± 2.4	47.2 ± 6.8	38.1 ± 7.4	52 ± 5	47.7 ± 3.9	58 ± 10.5
T50% peak shortening (ms)	75 ± 1	70 ± 3 ($P < 0.05$ vs. control)	75 ± 2	79 ± 1	83 ± 2	78 ± 2
T50 Ca^{2+} transient (ms)	161 ± 3	152 ± 5	164 ± 5	183 ± 5 ($P < 0.001$ vs. WT control)	179 ± 9	164 ± 8 ($P < 0.03$ vs. control)

Data represent mean ± SEM from at least 20 cells for each group isolated from at least four different hearts. T50% peak shortening, time from baseline to 50% peak shortening; T50 Ca^{2+} transient, time to 50% Ca^{2+} transient decay.

TABLE 2
Contractility and Ca^{2+} transient kinetics in ventricular myocytes isolated from WT and *db/db* mice, under HG in the presence of ISO (10 nmol/L), without and with Palm at two different concentrations

	Glucose 30 mmol/L + ISO					
	WT			*db/db*		
	Control	Palm 0.4 mmol/L	Palm 0.8 mmol/L	Control	Palm 0.4 mmol/L	Palm 0.8 mmol/L
FS (%)	8.99 ± 0.6	14.8 ± 0.7 ($P < 0.001$ vs. control)	10.8 ± 1.0	7.4 ± 0.7 ($P < 0.02$ vs. WT control)	14.1 ± 1.1 ($P < 0.001$ vs. control)	12.1 ± 1.3 ($P < 0.002$ vs. control)
Ca^{2+} transient (%)	44.7 ± 2.9	64.6 ± 5.3 ($P < 0.05$ vs. control)	50.9 ± 5.8	49 ± 3.6	43.8 ± 4.1	55 ± 9.7
T50% peak shortening (ms)	78 ± 1	69 ± 1 ($P < 0.001$ vs. control)	74 ± 1	80 ± 1	78 ± 1	74 ± 1 ($P < 0.01$ vs. control)
T50 Ca^{2+} transient (ms)	159 ± 2	150 ± 2	147 ± 6	181 ± 5 ($P < 0.001$ vs. WT control)	175 ± 11	164 ± 7 ($P < 0.04$ vs. control)

Data represent mean ± SEM from at least 20 cells for each group isolated from at least four different hearts. T50% peak shortening, time from baseline to 50% peak shortening; T50 Ca^{2+} transient, time to 50% Ca^{2+} transient decay.

DISCUSSION

Here we show that energetically/redox-stressed cardiomyocytes from type 2 diabetic *db/db* mice display impaired mitochondrial state 4→3 energetic transition, accounting for uninhibited ROS emission, under both FET and RET modes. Deficits in local pools of mitochondrial GSH and Trx2 account for this amplified ROS emission. The resulting more-oxidizing intracellular environment correlates with altered E-C coupling in cardiomyocytes/intact hearts. These alterations are causative and not incidental because exogenous GSH rescues both mitochondrial/cellular redox balance and E-C coupling. Also, shifting substrates, i.e., the use of the FA Palm, reestablishes proper myocyte redox milieu while improving function in metabolically/redox-challenged whole hearts.

The balance between ROS production in the respiratory chain and the efficiency of the ROS scavenging systems determines mitochondrial H_2O_2 emission as a function of the redox environment (29). Here we assign to mitochondrial impairment in the key state 4→3 energetic transition, and defective mitochondrial GSH and Trx2 systems, a leading role in the excess ROS emission occurring in *db/db* myocytes, ultimately resulting in myocyte/whole-heart functional impairment. Uncoupling of OxPhos, along with the inability of mitochondria to decrease ROS levels during the state 4→3 transition under FET, plays a major role in the energetic/redox dysfunction. Recent data show that under states 4 and 3, mouse heart mitochondria divert a significant portion of total respiratory flow to ROS generation, which is continuously offset by GSH/Trx scavenging systems (30,33).

Indeed, HG + ISO provoked a concomitant rise in ROS levels and GSH depletion that was associated with contractile and Ca^{2+} handling failure. Mechanistically, the resetting of mitochondrial and cellular redox balance operated by exogenous GSH was mediated by the TrxR2/Trx2/peroxiredoxin 3 (Prx3) system, whose redox potential became more reduced in the presence of additional cytoplasmic GSH. The augmented scavenging capacity bestowed by GSHee could also indirectly increase SOD activity by lowering H_2O_2, which exerts a negative feedback on this enzyme (41) (Supplementary Fig. 4). Herein, intact ex vivo perfused *db/db* hearts exhibited altered vascular tone, impaired LV function, and significant shortening of APD compared with WT hearts. These deficits are all crucial for maintaining proper E-C coupling, and thus contraction, under both basal and increased-workload conditions. A possible mechanism responsible for APD shortening is the nonischemic activation of sarcolemmal ATP-sensitive (K-ATP) channels, reflecting energetic shortage when energy demand is high in *db/db* hearts. Impaired myocardial Ca^{2+} handling is known to be involved in diabetic cardiomyopathy (42). Our study shows that these alterations become particularly prominent when diabetic cells are subjected to redox/energetic stress, thus expanding previous observations showing that β-adrenergic response may be blunted in *db/db* myocytes (42,43).

The status of diabetic cardiomyopathy is maintained by the compounding effects of HG, mitochondrial energy deficit, and oxidative stress. However, no major contractile deficits are evident under HG alone, even in *db/db* hearts. This prompted us to use conditions of combined energetic/redox challenge (44). Since myocardial glucose metabolism (e.g., transport and glycolysis) is decreased and FA oxidation increased in diabetes (11), we analyzed the effect of the saturated FA Palm on intracellular redox, contractility, and Ca^{2+} handling in myocytes/hearts. Palm determined a transition from oxidized-to-reduced cellular redox status in *db/db* cardiomyocytes, abating ROS levels drastically. This effect was coupled to a marked GSH rise both in WT and *db/db* myocytes (Fig. 2*B*). Consequently, Palm significantly improved ISO-induced contractile reserve in *db/db* cardiomyocytes. Conversely, its absence was accompanied by marked deficits in Ca^{2+} handling and myocyte mechanical properties (Fig. 5*A–D*). Myocardial substrate use in patients with diabetes involves increased delivery of FAs (3,11,45). At the whole-heart level, Palm produced a substantial improvement in LV function in *db/db* hearts exposed to metabolic/redox stress, and a relative decrease in the WT. Previous reports have elegantly shown that, in the presence of 11 mmol/L glucose, Palm has a negative impact on LV function of *db/db* mice (25). Present evidence is consistent with these findings, and may help to mechanistically explain the decline in LV function and efficiency seen in *db/db* hearts with

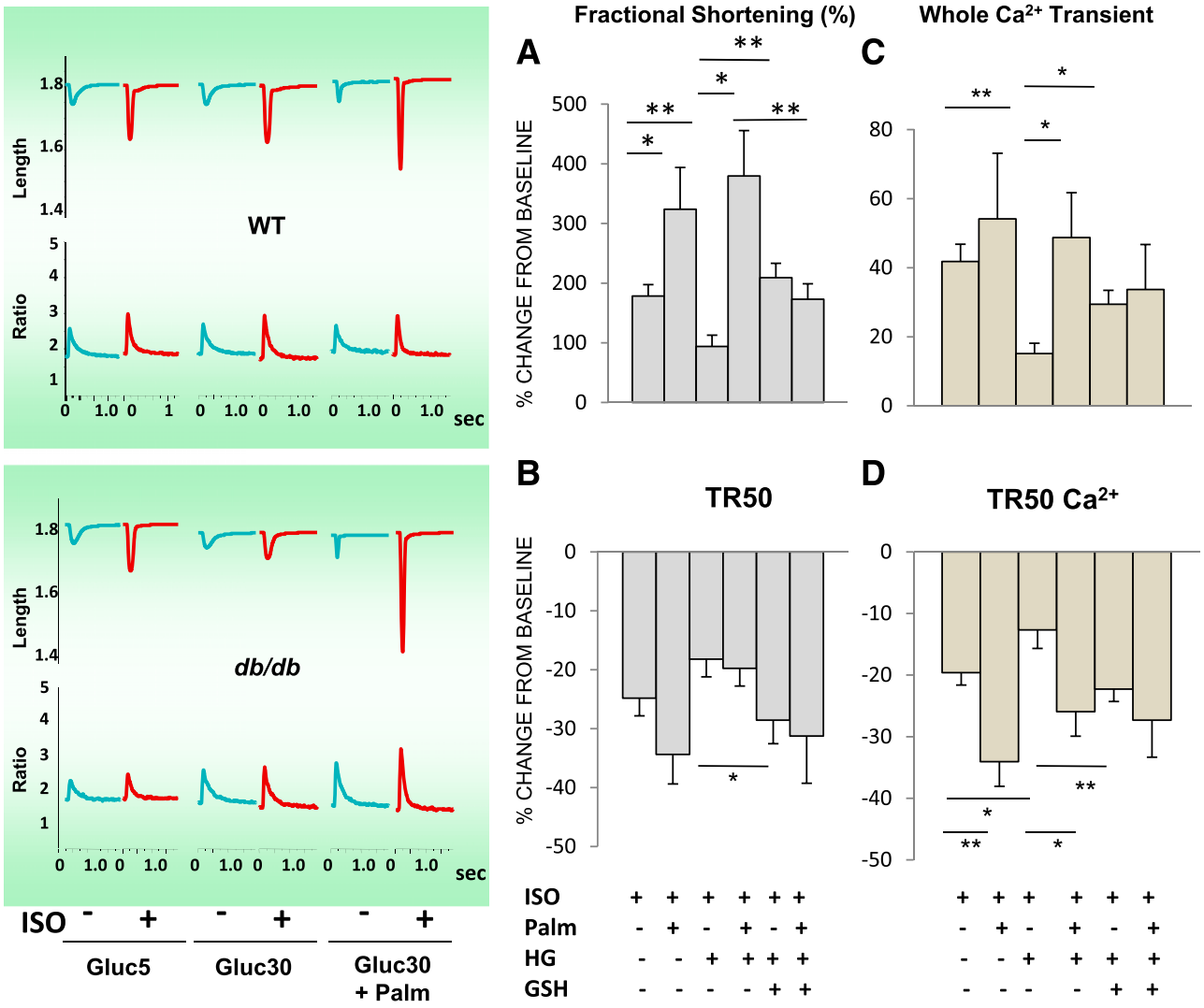

FIG. 5. Contractile behavior of *db/db* cardiomyocytes under EG and hyperglycemia without or with β-adrenergic stimulation and GSHee or Palm preincubation. Cardiomyocytes from *db/db* mouse hearts were isolated, handled, and analyzed for cell shortening (*A* and *C*) and Ca^{2+} transients (*B* and *D*), in parallel with the imaging studies (Fig. 2). *Left*: Representative traces of the main experimental situations. EG and HG were used in the absence or presence of β-adrenergic stimulation with 10 nmol/L ISO and without or with preincubation in the presence of 4 mmol/L GSHee for 3 h or Palm (0.4 or 0.8 mmol/L for WT and *db/db*, respectively), at room temperature (Tables 1 and 2). The number of samples analyzed was n = 20–30 (from four to six hearts). T50% peak shortening, from baseline to 50% peak shortening; TR50, time to 50% relengthening; T50 Ca^{2+}, time to 50% Ca^{2+} transient decay. *$P < 0.05$; **$P < 0.01$.

Palm + glucose (25). However, here we aimed to test a different question, i.e., how isolated *db/db* myocytes/hearts respond to increased metabolic/redox stress using the HG + ISO regimen. Although Palm partially worsened LV function in WT hearts, it definitely improved the performance of *db/db* hearts subjected to HG + ISO. Thus, our study suggests that in animals with type 2 diabetes, FAs are important for handling increased workload that demands higher energy supply while exposing cardiac tissue to the likelihood of ROS imbalance (46).

FAs are a major source of acetyl-coenzyme A for the tricarboxylic acid cycle, contributing 60–70% of myocardial ATP at physiological levels (40). However, the higher energetic budget provided by Palm (three times higher than from glucose) is produced up to two-thirds in the form of reducing equivalents (24 NADH and 8 $FADH_2$) from β-oxidation in mitochondria. This reducing power contributes electrons to antioxidant systems and the mitochondrial respiratory/energetic machinery (Fig. 1). The significantly lower levels of GSH found in *db/db* cardiomyocytes argue in favor of a more oxidized and constitutively compromised supply of reducing equivalents to the GSH/Trx systems through NADPH (Fig. 1). The rescue of $Trx(SH)_2$ to WT levels via GSHee supports this contention, suggesting that the achievement of a more balanced redox status could be mediated by the TrxR2/Trx2/Prx3 pathway, a major controller of H_2O_2 emission from mitochondria (30,33). The recovery of contractile activity observed in *db/db* cardiomyocytes preincubated with GSHee, along with a more-reduced redox status in cells, and of Trx2 in mitochondria, demonstrates for the first time that changes in mitochondrial pools of GSH and Trx2 can have a negative impact that propagates from mitochondria to the function of myocytes in challenged *db/db* hearts.

Concerning the role of FAs, one intrinsic limitation of our study is that we tested only the acute effects of Palm. In a more chronic stand, the upregulation of FA uptake is

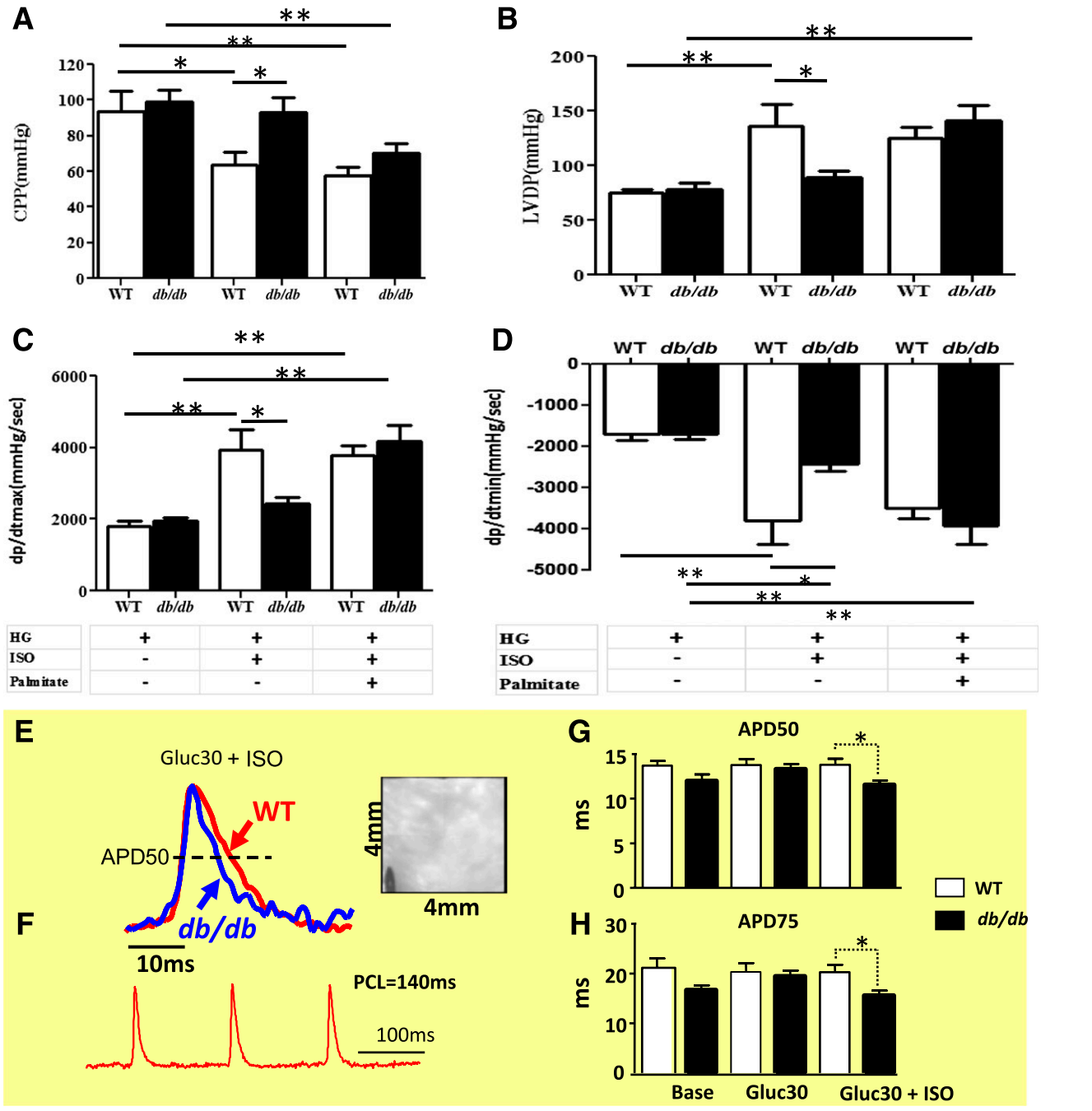

FIG. 6. LV function in Langendorff-perfused hearts and high-resolution optical AP imaging. Hearts were harvested, handled, and perfused as described in RESEARCH DESIGN AND METHODS. Hearts were paced with a Radnoti pacing electrode (Monrovia, CA) at 600 bpm (10 Hz, 4-ms duration, 4 V) using a Grass stimulator (Grass Instruments Co., Quincy, MA). LV function was monitored with a water-filled, customized latex balloon connected to a P23XL pressure transducer with interface cable (Harvard Apparatus Instruments, Holliston, MA) and coupled to a BIOPAC System (DA100, Santa Barbara, CA) for continuous data recording and offline analysis. LV end-diastolic pressure was set at 5–10 mmHg by adjusting the balloon volume with a Gilmont micrometer syringe (Cole-Parmer, Vernon Hills, IL). After stabilization in KH buffer (11 mmol/L glucose; EG), the heart was exposed to ISO (10 nmol/L), followed by a drug-free perfusion period to recover baseline parameters. The same heart was perfused for 1 h with KH buffer containing 30 mmol/L glucose, followed by exposure to ISO again. Shown are (in mmHg) the CPP, LVDP, and (in mmHg/s) maximal rates of contraction (dP/dt_{max}) and relaxation (dP/dt_{min}) observed under HG (30 mmol/L glucose), in the absence or presence of ISO (10 nmol/L) and Palm (WT, 0.4 mmol/L; *db/db*, 0.8 mmol/L). The data presented correspond to n = 4 hearts in each group of WT or *db/db*. The same protocol was applied at Palm 0.2 mmol/L WT and 0.4 mmol/L *db/db* under EG and HG (n = 6 hearts from each group; see Supplementary Figs. 5–7). APD was measured in paced (140-ms pacing cycle length [PCL]) WT and *db/db* hearts during perfusion under baseline, HG, and HG + ISO. The CCD-based, high-resolution optical mapping system is capable of measuring APs from 6,400 pixels of the 4 × 4-mm^2 epicardial surface with high temporal (1 ms) and spatial (50 μm) resolutions in intact murine hearts. Also measured were epicardial conduction velocity (CV) and normalized AP upstroke velocity under the same conditions (Supplementary Fig. 8). *E* and *F*: Representative epicardial APs measured from WT (red) and *db/db* (blue) mice during pacing at 140 ms PCL. Also shown is a CCD-based image of the mapped epicardial region with the pacing electrode in the lower left corner. *G* and *H*: The HG + ISO regimen uncovered a significant shortening of APD50 and APD75 in *db/db* but not WT hearts. *P < 0.05; **P < 0.01.

known to promote the accumulation of intracellular lipid, resulting in lipotoxic effects (47), likely due to deficits in lipase function, ultimately leading to cardiac disease (11,25). Notwithstanding, our findings suggest that, when properly used, FAs are important suppliers of reducing equivalents, particularly when *db/db* myocytes/hearts are exposed to HG and more workload.

ACKNOWLEDGMENTS

This work was supported by National Institutes of Health Grant R01-HL-091923-01. C.G.T. was supported by International Society for Heart Research–European Section/Servier; V.C. by Coordenação de Aperfeiçoamento de Pessoal de Nível Superior (CAPES), Brazil; and S.S. by the National Natural Science Foundation of China Grant 81100155.

No potential conflicts of interest relevant to this article were reported.

C.G.T., V.C., B.A.S., C.X., and S.S. researched data and contributed to discussion. W.H.W., B.O., and R.C.S.-B. contributed to discussion and reviewed and edited the manuscript. S.C. and F.G.A. researched data, contributed to discussion, and reviewed and edited the manuscript. N.P. and M.A.A. researched data, contributed to discussion, and wrote the manuscript. M.A.A. is the guarantor of this work and, as such, had full access to all the data in the study and takes responsibility for the integrity of the data and the accuracy of the data analysis.

Parts of this study were presented as a poster at the 54th Annual Meeting of the Biophysical Society, San Francisco, California, 20–24 February 2010; 55th Annual Meeting of the Biophysical Society, Baltimore, Maryland, 5–9 March 2011; and 56th Annual Meeting of the Biophysical Society, San Diego, California, 25–29 February 2012.

REFERENCES

1. Bell DSH. Heart failure: the frequent, forgotten, and often fatal complication of diabetes. Diabetes Care 2003;26:2433–2441
2. Laakso M. Hyperglycemia and cardiovascular disease in type 2 diabetes. Diabetes 1999;48:937–942
3. Boudina S, Abel ED. Diabetic cardiomyopathy, causes and effects. Rev Endocr Metab Disord 2010;11:31–39
4. Cohen-Solal A, Beauvais F, Logeart D. Heart failure and diabetes mellitus: epidemiology and management of an alarming association. J Card Fail 2008;14:615–625
5. Bruce DG, Chisholm DJ, Storlien LH, Kraegen EW, Smythe GA. The effects of sympathetic nervous system activation and psychological stress on glucose metabolism and blood pressure in subjects with type 2 (non-insulin-dependent) diabetes mellitus. Diabetologia 1992;35:835–843
6. Colberg SR, Albright AL, Blissmer BJ, et al. Exercise and type 2 diabetes: American College of Sports Medicine and the American Diabetes Association: joint position statement. Exercise and type 2 diabetes. Med Sci Sports Exerc 2010;42:2282–2303
7. Fang ZY, Sharman J, Prins JB, Marwick TH. Determinants of exercise capacity in patients with type 2 diabetes. Diabetes Care 2005;28:1643–1648
8. Dobrin JS, Lebeche D. Diabetic cardiomyopathy: signaling defects and therapeutic approaches. Expert Rev Cardiovasc Ther 2010;8:373–391
9. McGarry JD. What if Minkowski had been ageusic? An alternative angle on diabetes. Science 1992;258:766–770
10. Wisneski JA, Gertz EW, Neese RA, Mayr M. Myocardial metabolism of free fatty acids. Studies with 14C-labeled substrates in humans. J Clin Invest 1987;79:359–366
11. Lopaschuk GD, Ussher JR, Folmes CD, Jaswal JS, Stanley WC. Myocardial fatty acid metabolism in health and disease. Physiol Rev 2010;90:207–258
12. Cryer PE. Disorders of sympathetic neural function in human diabetes mellitus: hypoadrenergic and hyperadrenergic postural hypotension. Metabolism 1980;29(Suppl. 1):1186–1189
13. Huggett RJ, Scott EM, Gilbey SG, Stoker JB, Mackintosh AF, Mary DA. Impact of type 2 diabetes mellitus on sympathetic neural mechanisms in hypertension. Circulation 2003;108:3097–3101
14. Sivitz WI, Yorek MA. Mitochondrial dysfunction in diabetes: from molecular mechanisms to functional significance and therapeutic opportunities. Antioxid Redox Signal 2010;12:537–577
15. Styskal J, Van Remmen H, Richardson A, Salmon AB. Oxidative stress and diabetes: what can we learn about insulin resistance from antioxidant mutant mouse models? Free Radic Biol Med 2012;52:46–58
16. Maechler P, Jornot L, Wollheim CB. Hydrogen peroxide alters mitochondrial activation and insulin secretion in pancreatic beta cells. J Biol Chem 1999;274:27905–27913
17. Friederich M, Hansell P, Palm F. Diabetes, oxidative stress, nitric oxide and mitochondria function. Curr Diabetes Rev 2009;5:120–144
18. Choi SW, Benzie IF, Ma SW, Strain JJ, Hannigan BM. Acute hyperglycemia and oxidative stress: direct cause and effect? Free Radic Biol Med 2008;44:1217–1231
19. Evans JL, Goldfine ID, Maddux BA, Grodsky GM. Oxidative stress and stress-activated signaling pathways: a unifying hypothesis of type 2 diabetes. Endocr Rev 2002;23:599–622
20. Brownlee M. Advanced protein glycosylation in diabetes and aging. Annu Rev Med 1995;46:223–234
21. Lowell BB, Shulman GI. Mitochondrial dysfunction and type 2 diabetes. Science 2005;307:384–387
22. Akar FG, Aon MA, Tomaselli GF, O'Rourke B. The mitochondrial origin of postischemic arrhythmias. J Clin Invest 2005;115:3527–3535
23. Aon MA, Cortassa S, Akar FG, Brown DA, Zhou L, O'Rourke B. From mitochondrial dynamics to arrhythmias. Int J Biochem Cell Biol 2009;41:1940–1948
24. Slodzinski MK, Aon MA, O'Rourke B. Glutathione oxidation as a trigger of mitochondrial depolarization and oscillation in intact hearts. J Mol Cell Cardiol 2008;45:650–660
25. Boudina S, Sena S, Theobald H, et al. Mitochondrial energetics in the heart in obesity-related diabetes: direct evidence for increased uncoupled respiration and activation of uncoupling proteins. Diabetes 2007;56:2457–2466
26. Anderson EJ, Lustig ME, Boyle KE, et al. Mitochondrial H2O2 emission and cellular redox state link excess fat intake to insulin resistance in both rodents and humans. J Clin Invest 2009a;119:573–581
27. Ren J, Pulakat L, Whaley-Connell A, Sowers JR. Mitochondrial biogenesis in the metabolic syndrome and cardiovascular disease. J Mol Med (Berl) 2010;88:993–1001
28. Buchanan J, Mazumder PK, Hu P, et al. Reduced cardiac efficiency and altered substrate metabolism precedes the onset of hyperglycemia and contractile dysfunction in two mouse models of insulin resistance and obesity. Endocrinology 2005;146:5341–5349
29. Aon MA, Cortassa S, O'Rourke B. Redox-optimized ROS balance: a unifying hypothesis. Biochim Biophys Acta 2010b;1797:865–877
30. Aon MA, Stanley BA, Sivakumaran V, et al. Glutathione/thioredoxin systems modulate mitochondrial H2O2 emission: an experimental-computational study. J Gen Physiol 2012;139:479–491
31. Aon MA, Cortassa S, Maack C, O'Rourke B. Sequential opening of mitochondrial ion channels as a function of glutathione redox thiol status. J Biol Chem 2007;282:21889–21900
32. Tocchetti CG, Wang W, Froehlich JP, et al. Nitroxyl improves cellular heart function by directly enhancing cardiac sarcoplasmic reticulum Ca2+ cycling. Circ Res 2007;100:96–104
33. Stanley BA, Sivakumaran V, Shi S, et al. Thioredoxin reductase-2 is essential for keeping low levels of H(2)O(2) emission from isolated heart mitochondria. J Biol Chem 2011;286:33669–33677
34. Go Y-M, Jones DP. Thioredoxin redox Western analysis. Current Protocols in Toxicology 2009;17.12(Suppl. 41):1–12
35. Roepke TK, Kontogeorgis A, Ovanez C, et al. Targeted deletion of kcne2 impairs ventricular repolarization via disruption of I(K,slow1) and I(to,f). FASEB J 2008;22:3648–3660
36. Akar FG, Tomaselli GF. Conduction abnormalities in nonischemic dilated cardiomyopathy: basic mechanisms and arrhythmic consequences. Trends Cardiovasc Med 2005;15:259–264
37. Boardman N, Hafstad AD, Larsen TS, Severson DL, Aasum E. Increased O2 cost of basal metabolism and excitation-contraction coupling in hearts from type 2 diabetic mice. Am J Physiol Heart Circ Physiol 2009;296:H1373–H1379
38. Schönfeld P, Wojtczak L. Fatty acids as modulators of the cellular production of reactive oxygen species. Free Radic Biol Med 2008;45:231–241
39. Wei AC, Aon MA, O'Rourke B, Winslow RL, Cortassa S. Mitochondrial energetics, pH regulation, and ion dynamics: a computational-experimental approach. Biophys J 2011;100:2894–2903
40. Lopaschuk GD. Metabolic abnormalities in the diabetic heart. Heart Fail Rev 2002;7:149–159

41. Cortassa S, Aon MA, Winslow RL, O'Rourke B. A mitochondrial oscillator dependent on reactive oxygen species. Biophys J 2004;87:2060–2073
42. Belke DD, Dillmann WH. Altered cardiac calcium handling in diabetes. Curr Hypertens Rep 2004;6:424–429
43. Pereira L, Matthes J, Schuster I, et al. Mechanisms of [Ca2+]i transient decrease in cardiomyopathy of db/db type 2 diabetic mice. Diabetes 2006;55:608–615
44. Bahmani F, Bathaie SZ, Aldavood SJ, Ghahghaei A. Glycine therapy inhibits the progression of cataract in streptozotocin-induced diabetic rats. Mol Vis 2012;18:439–448
45. Leone TC, Kelly DP. Transcriptional control of cardiac fuel metabolism and mitochondrial function. Cold Spring Harb Symp Quant Biol 2011 76:175–182
46. Kohlhaas M, Liu T, Knopp A, et al. Elevated cytosolic Na+ increases mitochondrial formation of reactive oxygen species in failing cardiac myocytes. Circulation 2010;121:1606–1613
47. Brookheart RT, Michel CI, Schaffer JE. As a matter of fat. Cell Metab 2009;10:9–12
48. Chance B, Williams GR. Respiratory enzymes in oxidative phosphorylation. III. The steady state. J Biol Chem 1955;217:409–427
49. Nicholls DG, Ferguson SJ. *Bioenergetics 3*. London, San Diego, Academic Press, 2002